Lattice Boltzmann model for the convection-diffusion equation

Zhenhua Chai and T. S. Zhao

A new lattice Boltzmann model for the convection-diffusion equation

Zhenhua Chai, T. S. Zhao[*]

Department of Mechanical Engineering

The Hong Kong University of Science and Technology, Clear Water Bay, Kowloon

Hong Kong SAR, People's Republic of China

We propose a new lattice Boltzmann (LB) model for the convection-diffusion equation (CDE) and show that the CDE can be recovered correctly from the model by the Chapman-Enskog analysis. The most striking feature of the present LB model is that it enables the collision process to be implemented locally, making it possible to retain the advantage of the lattice Boltzmann method in the study of the heat and mass transfer in complex geometries. A local scheme for computing the heat and mass fluxes is then proposed to replace conventional nonlocal finite-difference schemes. We further validate the present model and the local scheme for computing the flux against analytical solutions to several classical problems, and show that both the model for the CDE and the computational scheme for the flux have a second-order convergence rate in space. It is also demonstrated the present model is more accurate than existing LB models for the CDE.

PACS number(s): 47.11.-j, 44.05.+e

---

[*] Corresponding author: metzhao@ust.hk

I. Introduction

The convection-diffusion or advection-diffusion equation is widely used to describe transport phenomena where heat, mass and other physical quantities are transferred due to the diffusion and advection processes [1]. The equation is given by:

$$\frac{\partial \phi}{\partial t} + \nabla \cdot (\phi \mathbf{u}) = \nabla \cdot (D \nabla \phi),\tag{1}$$

where ϕ represents a scalar variable and is a function of both time and space, D is the diffusion coefficient. $\mathbf{u}$ is the velocity, and governed by the incompressible Navier-Stokes (N-S) equations:

$$\nabla \cdot \mathbf{u} = 0,\tag{2}$$

$$\frac{\partial \mathbf{u}}{\partial t} + \mathbf{u} \cdot \nabla \mathbf{u} = -\frac{1}{\rho} \nabla P + \nu \nabla^2 \mathbf{u} + \mathbf{a},\tag{3}$$

where P is the pressure, ρ is the fluid density, ν is the kinematic viscosity, and $\mathbf{a}$ is the acceleration due to external force.

To reveal transport phenomena governed by the CDE, the best way is to obtain an exact solution with a suitable analytical method, but it has proven very difficult as the velocity in the CDE is coupled with the N-S equations (2) and (3). For this reason, many numerical approaches, including the finite-difference, finite-volume and finite-element methods, have been developed [2-4]. However, these methods are challenging in the study of the mass or heat transfer in a complex geometry (e.g., porous media).

The lattice Boltzmann method (LBM), as a kinetic based numerical method, has made a great progress in the study of fluid flows for its advantage in dealing with complex boundaries [5-9], and has also been extended to solve the CDE [10-22]. Dawson et al. [10] first applied the LBM to the study of solvent flow where an LB model was used to solve

the N-S equations for fluid flow, while another was adopted to solve the CDE for the concentration field; the method has also been extended to investigate thermal flows [11]. To improve the efficiency of the LBM for CDE, van der Sman and Ernst [12] developed an LB model with irregular lattices, which may be more efficient for some special physical problems. In addition, they also compared the LBM with some traditional methods (finite-difference and finite-element methods), and found that the LBM had a comparable performance with these traditional approaches. Shi and co-workers [13, 14] proposed a new LB model for the CDE with a source term; unlike some previous models, an additional term is included in this model such that the CDE with a source term can be recovered. Zhang et al. [15] constructed an LB model for the anisotropic CDE in which the Bhatnagar-Gross-Krook (BGK) collision operator and a directionally dependent relaxation time for each pair distribution function with opposite discrete velocities are used. However, as pointed out by Ginzburg [16], this BGK-typed LB model cannot have a mass conserving equilibrium distribution function once the relaxation times differ with each other. To overcome this problem inherent in the BGK-typed LB model, the two-relaxation-time and multiple-relaxation-time LB models have also been proposed in a more general way to solve the anisotropic CDE [16-19]. Although many LB models have been proposed for the CDE, the Chapman-Enskog analysis shows that the CDE can only be recovered exactly from these models under some unrealistic assumptions (e.g., the velocity must be a constant). However, these assumptions adopted in these previous works may not be satisfied in practice and also influence the accuracy of the lattice Boltzmann model [20]. Generally speaking, there are two possible ways that can be used to eliminate constrains of the assumptions adopted in these available LB models. The first

is to add a source term in the evolution equation of the LB model such that the CDE can be recovered correctly [20]. Chopard et al. [20] used this method to construct an LB model for CDE, in which a time-derivative or space-derivative term is added in the evolution equation, and found that the model with the space-derivative term is more accurate. However, the collision process of the model with the space-derivative term cannot be implemented locally (here the word 'local' means that the computation of a physical variable at one point only depends on the information of this point) since a finite-difference scheme is needed to compute the space-derivative term, which not only affects the computational efficiency of the lattice Boltzmann method, but also gives rise to some difficulties in adopting a local scheme to treat the boundary condition of the CDE. The other is to construct an LB model with a modified evolution equation (without adding a source term in the evolution equation) to ensure that the unwanted terms in the previous models can be eliminated completely [21, 22]. However, the collision process cannot yet be performed locally, and thus the problems mentioned above still remain.

To address the above mentioned problems in previous LB models for the CDE, this work reports a new LB model that makes use of a modified equilibrium distribution function and the evolution equation with a source term. The Chapman-Enskog analysis shows that the CDE can be recovered exactly from the new model. More importantly, the model enables the collision process to be implemented locally. In the following, we present the model first, followed by the Chapman-Enskog analysis to recover the CDE. With this model, we then present a local scheme, instead of the traditionally nonlocal finite-difference schemes, to compute the heat and mass fluxes. Finally, some numerical examples are carried out to test the present model and the scheme in computing the flux.

The numerical results show that both the present model for CDE and the local scheme in computing the flux have a second-order convergence rate in space.

II. Model Development

The lattice Boltzmann method can be viewed as a mesoscopic numerical approach for computational fluid dynamics [7] and a general solver to some special partial differential equations [23-26]. Based on the collision operator, the models of LBM can be classified into three groups: the single-relaxation-time model (or so called BGK model) [27], the two-relaxation-time model [28], and the multiple-relaxation-time model [29, 30]. In this work, the BGK model is considered for its simplicity and high computational efficiency. The evolution equation of the BGK model for the CDE, given by Eq. (1), can be written as [20]:

$$\phi_i\left(\mathbf{x}+\mathbf{c}_i\delta t,\, t+\delta t\right)-\phi_i\left(\mathbf{x},\, t\right)=-\frac{1}{\tau_\phi}\left[\phi_i\left(\mathbf{x},\, t\right)-\phi_i^{(eq)}\left(\mathbf{x},\, t\right)\right]+R_i\left(\mathbf{x},\, t\right),\qquad(4)$$

which includes the two separate steps, i.e., collision and propagation,

$$\text{Collision:}\ \phi_i^+\left(\mathbf{x},\, t\right)=\phi_i\left(\mathbf{x},\, t\right)-\frac{1}{\tau_\phi}\left[\phi_i\left(\mathbf{x},\, t\right)-\phi_i^{(eq)}\left(\mathbf{x},\, t\right)\right]+R_i\left(\mathbf{x},\, t\right),\qquad(5)$$

$$\text{Propagation:}\ \phi_i\left(\mathbf{x}+\mathbf{c}_i\delta t,\, t+\delta t\right)=\phi_i^+\left(\mathbf{x},\, t\right),\qquad(6)$$

where $\phi_i\left(\mathbf{x},\, t\right)$ and $\phi_i^+\left(\mathbf{x},\, t\right)$ are the distribution function and post-collision distribution function associated with velocity $\mathbf{c}_i$ at position $\mathbf{x}$ and time t, τ_ϕ is the dimensionless relaxation time. $\phi_i^{(eq)}\left(\mathbf{x},\, t\right)$ is local equilibrium distribution function, and defined by:

$$\phi_i^{(eq)}=w_i\phi\left[1+\frac{\mathbf{c}_i\cdot\mathbf{u}}{c_s^2}+\frac{\left(\mathbf{c}_i\cdot\mathbf{u}\right)^2}{2c_s^4}-\frac{\mathbf{u}\cdot\mathbf{u}}{2c_s^2}\right]+\lambda_i\frac{\phi P}{\rho_0 c_s^2},\qquad(7)$$

5

where ρ_0 is the average value of the fluid density ρ, w_i and λ_i are weight coefficients,

and satisfy the following conditions:

$$\sum_i w_i = 1, \quad \sum_i \lambda_i = 0,$$

$$\sum_i w_i \mathbf{c}_{i,\alpha} = \sum_i \lambda_i \mathbf{c}_{i,\alpha} = 0,$$

$$\sum_i w_i \mathbf{c}_{i,\alpha} \mathbf{c}_{i,\beta} = \sum_i \lambda_i \mathbf{c}_{i,\alpha} \mathbf{c}_{i,\beta} = c_s^2 \delta_{\alpha\beta}, \tag{8}$$

$$\sum_i w_i \mathbf{c}_{i,\alpha} \mathbf{c}_{i,\beta} \mathbf{c}_{i,\gamma} = \sum_i \lambda_i \mathbf{c}_{i,\alpha} \mathbf{c}_{i,\beta} \mathbf{c}_{i,\gamma} = 0,$$

$$\sum_i w_i \mathbf{c}_{i,\alpha} \mathbf{c}_{i,\beta} \mathbf{c}_{i,\gamma} \mathbf{c}_{i,\theta} = \sum_i \lambda_i \mathbf{c}_{i,\alpha} \mathbf{c}_{i,\beta} \mathbf{c}_{i,\gamma} \mathbf{c}_{i,\theta} = \Delta_{\alpha\beta\gamma\theta},$$

where $\Delta_{\alpha\beta\gamma\theta} = \delta_{\alpha\beta}\delta_{\gamma\theta} + \delta_{\alpha\gamma}\delta_{\beta\theta} + \delta_{\alpha\theta}\delta_{\beta\gamma}$, $\delta_{\alpha\beta}$ is the Kronecker delta with two indices. For

simplicity but without the loss of generality, the weight coefficient λ_i is set as

$\lambda_0 = -\sum_{i \neq 0} \lambda_i$, $\lambda_i = w_i \, (i \neq 0)$. $\mathbf{c}_i$ is the discrete velocity, and can be found in some

published works (e.g., [27]). R_i is the source term, and given by:

$$R_i(\mathbf{x}, t) = w_i \left(1 - \frac{1}{2\tau_\phi}\right) \delta t \frac{\mathbf{c}_i \cdot (P \nabla \phi / \rho_0 + \phi \, \mathbf{a})}{c_s^2}. \tag{9}$$

Based on mass conservation and Eq. (8), ϕ_i and $\phi_i^{(eq)}$ should satisfy the following

equations:

$$\phi = \sum_i \phi_i = \sum_i \phi_i^{(eq)}, \tag{10}$$

$$\phi \, \mathbf{u} = \sum_i \mathbf{c}_i \phi_i^{(eq)}. \tag{11}$$

It should be noted that a linear equilibrium distribution function has also been widely

used in previous LB models for CDE [11, 15 ,16, 20], which, however, leads to a

numerical diffusion coefficient in the recovered CDE [16, 20]. As the numerical diffusion

coefficient is proportional to the square of the velocity, the LB model with the linear equilibrium distribution function will result in lager errors in solving the CDE [20].

We now perform the Chapman-Enskog analysis to derive the CDE from the present model. To this end, we first expand the distribution function ϕ_i, the derivatives of time and space, and the acceleration $\mathbf{a}$ as [6, 32]:

$$\phi_i = \phi_i^{(0)} + \varepsilon \phi_i^{(1)} + \varepsilon^2 \phi_i^{(2)} + \dots, \tag{12a}$$

$$\frac{\partial}{\partial t} = \varepsilon \frac{\partial}{\partial t_1} + \varepsilon^2 \frac{\partial}{\partial t_2}, \tag{12b}$$

$$\nabla = \varepsilon \nabla_1, \tag{12c}$$

$$\mathbf{a} = \varepsilon \mathbf{a}_1. \tag{12d}$$

Appling the Taylor expansion to Eq. (4), we obtain:

$$\delta t \left(\frac{\partial}{\partial t} + \mathbf{c}_i \cdot \nabla \right) \phi_i + \frac{\delta t^2}{2} \left(\frac{\partial}{\partial t} + \mathbf{c}_i \cdot \nabla \right)^2 \phi_i = -\frac{1}{\tau_\phi} \left[\phi_i - \phi_i^{(eq)} \right] + R_i. \tag{13}$$

Substituting Eqs. (12) into Eq. (13), one can derive the zero, first, and second-order equations in ε as:

$$\varepsilon^0: \qquad \phi_i^{(0)} = \phi_i^{(eq)}, \tag{14a}$$

$$\varepsilon^1: \qquad \left(\frac{\partial}{\partial t_1} + \mathbf{c}_i \cdot \nabla_1 \right) \phi_i^{(0)} = -\frac{1}{\tau_\phi \delta t} \phi_i^{(1)} + w_i \left(1 - \frac{1}{2\tau_\phi} \right) \frac{\mathbf{c}_i \cdot \left(P \nabla_1 \phi / \rho_0 + \phi \mathbf{a}_1 \right)}{c_s^2}, \tag{14b}$$

$$\varepsilon^2: \qquad \frac{\partial \phi_i^{(0)}}{\partial t_2} + \left(\frac{\partial}{\partial t_1} + \mathbf{c}_i \cdot \nabla_1 \right) \phi_i^{(1)} + \frac{\delta t}{2} \left(\frac{\partial}{\partial t_1} + \mathbf{c}_i \cdot \nabla_1 \right)^2 \phi_i^{(0)} = -\frac{1}{\tau_\phi \delta t} \phi_i^{(2)}. \tag{14c}$$

From Eqs. (14a) and (14b) one can easily obtain:

$$\sum_i \phi_i^{(k)} = 0, \qquad k \geq 1, \tag{15}$$

$$\sum_i \mathbf{c}_i \phi_i^{(1)} = -\tau_\phi \delta t \left[\frac{\partial (\phi \mathbf{u})}{\partial t_1} + \nabla_1 \cdot \left(\phi c_s^2 \mathbf{I} + \phi \mathbf{u}\mathbf{u} + \frac{P}{\rho_0} \phi \mathbf{I} \right) - \left(1 - \frac{1}{2\tau_\phi} \right) (P\nabla_1 \phi / \rho_0 + \phi \mathbf{a}_1) \right], \quad (16)$$

where Eqs. (8) and (10) have been used.

Multiplying the operator $\partial / \partial t_1 + \mathbf{c}_i \cdot \nabla_1$ on the both sides of Eq. (14b), and substituting the result into Eq. (14c), we have:

$$\varepsilon^2 : \frac{\partial \phi_i^{(0)}}{\partial t_2} + \left(\frac{\partial}{\partial t_1} + \mathbf{c}_i \cdot \nabla_1 \right) \left(1 - \frac{1}{2\tau_\phi} \right) \left[\phi_i^{(1)} + \delta t w_i \frac{\mathbf{c}_i \cdot (P\nabla_1 \phi / \rho_0 + \phi \, \mathbf{a}_1)}{2c_s^2} \right] = -\frac{1}{\tau_\phi \delta t} \phi_i^{(2)}. \quad (17)$$

Summing Eqs. (14b) and (17) over i, and utilizing Eqs. (15) and (16), one can obtain the first and second-order recovered equations in ε as:

$$\varepsilon^1 : \quad \frac{\partial \phi}{\partial t_1} + \nabla_1 (\phi \, \mathbf{u}) = 0, \quad (18a)$$

$$\varepsilon^2 : \quad \frac{\partial \phi}{\partial t_2} + \nabla_1 \cdot \left\{ \left(1 - \frac{1}{2\tau_\phi} \right) \left(-\tau_\phi \delta t \right) \left[\frac{\partial (\phi \mathbf{u})}{\partial t_1} + \nabla_1 \cdot \left(\phi c_s^2 \mathbf{I} + \phi \mathbf{u}\mathbf{u} + \frac{P}{\rho_0} \phi \mathbf{I} \right) \right. \right.$$
$$\left. \left. - \left(1 - \frac{1}{2\tau_\phi} \right) (P\nabla_1 \phi / \rho_0 + \phi \mathbf{a}_1) \right] \right\} + \frac{\delta t}{2} \nabla_1 \cdot \left[\left(1 - \frac{1}{2\tau_\phi} \right) (P\nabla_1 \phi / \rho_0 + \phi \mathbf{a}_1) \right] = 0 \quad (18b)$$

Based on the first-order incompressible Navier-Stokes equations in ε [31],

$$\varepsilon^1 : \quad \frac{\partial \mathbf{u}}{\partial t_1} + \mathbf{u} \cdot \nabla_1 \mathbf{u} = -\frac{1}{\rho_0} \nabla_1 P + \mathbf{a}_1, \quad (19)$$

Eq. (18b) can be rewritten as:

$$\varepsilon^2 : \quad \frac{\partial \phi}{\partial t_2} - \nabla_1 \cdot (D\nabla_1 \phi) = 0, \quad (20)$$

where Eq. (18a) has been used. By combining the results at t_1 and t_2 scales, i.e., Eq. (18a) and Eq. (20), we recover the CDE as:

$$\frac{\partial \phi}{\partial t} + \nabla \cdot (\phi \mathbf{u}) = \nabla \cdot [D\nabla \phi], \quad (21)$$

where D is the diffusion coefficient, and given by

$$D = c_s^2\left(\tau_\phi - \frac{1}{2}\right)\delta t. \tag{22}$$

The above Chapman-Enskog analysis clearly shows that the CDE can be recovered correctly from the present model, in which a modified equilibrium distribution function and an additional source term are used. We note that the models proposed by Chopard et al. [20] and Zheng et al. [22] can also be used to recover the CDE, but a problem within the previous models is that the collision processes cannot be implemented locally. To ensure the collision process, Eq. (5), of the present model to be performed locally, a local scheme, given by Eq. (31), is proposed to compute the gradient term $\nabla\phi$ appearing in the source term R_i [see Eq. (9)].

In addition to the lattice Boltzmann model for the CDE, we also need another lattice Boltzmann model to solve the N-S equations (2) and (3). In the present work, the model proposed by He and Luo [31] is adopted since it is more accurate in the study of incompressible flows. Similar to Eq. (4), the evolution of the model reads

$$f_i(\mathbf{x} + \mathbf{c}_i\delta t, t + \delta t) - f_i(\mathbf{x}, t) = -\frac{1}{\tau_f}\left[f_i(\mathbf{x}, t) - f_i^{(eq)}(\mathbf{x}, t)\right] + F_i(\mathbf{x}, t), \tag{23}$$

where $f_i(\mathbf{x}, t)$ is the distribution function, $f_i^{(eq)}(\mathbf{x}, t)$ is the equilibrium distribution function, and defined as

$$f_i^{(eq)} = w_i\left\{\rho + \rho_0\left[\frac{\mathbf{c}_i \cdot \mathbf{u}}{c_s^2} + \frac{(\mathbf{c}_i \cdot \mathbf{u})^2}{2c_s^4} - \frac{\mathbf{u} \cdot \mathbf{u}}{2c_s^2}\right]\right\}. \tag{24}$$

where the average fluid density ρ_0 is set to be 1.0 for simplicity. F_i is the forcing term, and given by [32]

$$F_i(\mathbf{x}, t) = w_i\left(1 - \frac{1}{2\tau_\phi}\right)\delta t\left[\frac{\mathbf{c}_i - \mathbf{u}}{c_s^2} + \frac{(\mathbf{c}_i \cdot \mathbf{u})}{c_s^2}\mathbf{c}_i\right] \cdot (\rho_0\mathbf{a}). \qquad (25)$$

The macroscopic density and velocity can be obtained from:

$$\rho = \sum_i f_i, \qquad (26)$$

$$\mathbf{u} = \frac{1}{\rho_0}\sum_i \mathbf{c}_i f_i + \frac{\delta t}{2}\mathbf{a}. \qquad (27)$$

Through the Chapman-Enskog expansion, we can obtain the incompressible N-S equations (2) and (3) with the kinematic viscosity $\nu = c_s^2(\tau_f - 1/2)\delta t$.

III. A local scheme for the heat and mass fluxes

As discussed in Section I, in developing LB models for the CDE, many previous investigators focused on the accuracy and convergence rate of the model in describing the scalar variable ϕ [12-21]. More recently, the heat or mass flux, as another important physical variable, has also received increasing attention in predicting effective physical properties of porous media [33]. However, to our knowledge, there is no a special discussion on this topic in the framework of LBM. To fill the gap, we provide a local scheme, instead of the traditionally nonlocal finite-difference schemes, to compute the heat and mass fluxes, and perform a numerical study on the convergence rate of the scheme.

A general mathematical definition of the heat or mass flux ($\mathbf{J}$) can be given as

$$\mathbf{J} = -D\nabla\phi + \phi\mathbf{u}. \qquad (28)$$

Based on the results reported elsewhere [6, 7, 34], both the scalar variable ϕ and velocity $\mathbf{u}$ have a second-order accuracy in space, and thus the flux should have a first-order

convergence rate according to Eq. (28). However, as shown below, the flux can be computed from the non-equilibrium part of the distribution function with a second-order convergence rate, which is similar to the computation of the strain rate tensor or shear stress in the LBM [35, 36].

Substituting Eq. (19) into Eq. (16), one can obtain:

$$\sum_i \mathbf{c}_i \phi_i^{(1)} = -\tau_\phi \delta t \left[\left(\frac{P}{2\tau_\phi \rho_0} + c_s^2 \right) \nabla_1 \phi + \frac{\phi \mathbf{a}_1}{2\tau_\phi} \right], \tag{29}$$

from which we can further derive the expression of $\nabla_1 \phi$

$$\nabla_1 \phi = -\frac{2\sum_i \mathbf{c}_i \phi_i^{(1)} + \delta t \phi \mathbf{a}_1}{\delta t \left(P/\rho_0 + 2\tau_\phi c_s^2 \right)}. \tag{30}$$

Multiplying ε on both sides of Eq. (30) and utilizing the relation $\varepsilon \phi_i^{(1)} \approx \phi_i - \phi_i^{(eq)}$ (we note that this approximation has been widely used to calculate the strain rate tensor or shear stress in the LBM [35, 36]), we can obtain the following scheme to compute the gradient term $\nabla \phi$,

$$\nabla \phi = -\frac{2\sum_i \mathbf{c}_i \left[\phi_i - \phi_i^{(eq)} \right] + \delta t \phi \mathbf{a}}{\delta t \left(P/\rho_0 + 2\tau_\phi c_s^2 \right)}. \tag{31}$$

It is clear that Eq. (31) is a local scheme in the computation of the gradient term $\nabla \phi$ without adopting any finite-difference schemes. Substituting Eq. (31) into Eq. (9), we can also give a local scheme to compute the source term R_i so that the collision process of the present LB model can be implemented locally. In addition, substituting Eq. (31) into Eq. (28), one can derive a local scheme to compute the flux:

$$J = D \frac{2\sum_i \mathbf{c}_i \left[\phi_i - \phi_i^{(eq)}\right] + \delta t \phi \mathbf{a}}{\delta t \left(P/\rho_0 + 2\tau_\phi c_s^2\right)} + \phi \mathbf{u}. \tag{32}$$

Here we would like to point out that, in the same way as the computation of the shear stress and strain rate tensor [35, 36], the flux can also be calculated by the non-equilibrium part of the distribution function. Certain remarks on some schemes for computing the flux are given below:

Remark I: In the standard LB model for the CDE [10, 34], we can also use the non-equilibrium part of the distribution function to derive the computational scheme for the flux,

$$J = D \frac{\sum_i \mathbf{c}_i \left[\phi_i - \phi_i^{(eq)}\right] + \delta t \tau_\phi \phi(\mathbf{a} - \nabla P/\rho_0)}{\delta t \tau_\phi c_s^2} + \phi \mathbf{u}, \tag{33}$$

which, however, cannot be computed locally. This is because, in the framework of LBM, only the pressure, rather than the pressure gradient term ∇P, can be computed directly based on the relationship between the density and pressure. For this reason, an additional finite-difference scheme is needed to compute the pressure gradient term ∇P.

Remark II: In the corrected model proposed by Chopard et al. [20], one can also obtain a similar scheme for computing the flux,

$$J = D \frac{2\sum_i \mathbf{c}_i \left[\phi_i - \phi_i^{(eq)}\right] + \delta t \phi(\mathbf{a} - \nabla P/\rho_0)}{2\delta t \tau_\phi c_s^2} + \phi \mathbf{u}. \tag{34}$$

Like Eq. (33), Eq. (34) is also a nonlocal scheme for computing the flux, as an additional finite-difference scheme to compute pressure gradient term ∇P is also needed.

Remark III: For a pure diffusion process, i.e., the velocity $\mathbf{u}$ is zero, there is no flow field effect on the scalar variable ϕ. For this reason, the physical variables related to flow

field, including the pressure P and acceleration $\mathbf{a}$, can be chosen arbitrarily, and set to be zero for simplicity. Thus we can obtain a simple local scheme for the flux,

$$\mathbf{J} = \left(1 - \frac{1}{2\tau_\phi}\right)\sum_i \mathbf{c}_i\left[\phi_i - \phi_i^{(eq)}\right], \tag{35}$$

which can also be derived from Eqs. (33) and (34).

IV. Results and discussion

To test the accuracies of the present model for CDE and the local scheme for computing the flux, this section presents some benchmark examples, including a one-dimensional periodic problem, the problem of diffusion in the Couette flow with wall injection, and the problem of diffusion in the Poiseuille flow. In simulations, the following convergent criterion was used for a steady problem to ensure that the numerical results reach steady state,

$$\frac{\sum_{\mathbf{x}}\left|\phi(\mathbf{x}, t) - \phi(\mathbf{x}, t - 100 \times \delta t)\right|}{\sum_{\mathbf{x}}\left|\phi(\mathbf{x}, t)\right|} < 1.0 \times 10^{-8}. \tag{36}$$

To test the convergence rate of the present model for CDE and the local scheme for the flux, the relative error (E) is used,

$$E_\theta = \frac{\sum_{\mathbf{x}}\left|\theta_a(\mathbf{x}, t) - \theta_n(\mathbf{x}, t)\right|}{\sum_{\mathbf{x}}\left|\theta_a(\mathbf{x}, t)\right|}, \tag{37}$$

where θ represents the scalar variable ϕ or one of elements of the flux $\mathbf{J}$, the subscripts a and n denote the analytical and numerical solutions. Unless otherwise stated, the half-way anti-bounce-back and bounce-back schemes are used to treat the boundary conditions of CDE and N-S equations since they are both local schemes, and have a

second-order convergence rate in space [34, 37]. In addition, it is also known that the lattice Boltzmann method is a second-order accurate approach in the study of fluid flows [6, 7, 37], and thus we only focus on the results of present model for CDE and the scheme in computing the flux, and do not present any results of LB model for fluid flows.

A. Numerical validations

To validate present model for the CDE and the scheme for computing flux, we performed simulations of a one-dimensional periodic problem, diffusion in the Couette flow with wall injection, and diffusion in the Poiseuille flow, and compared the numerical results with the corresponding analytical solutions.

1. A one-dimensional periodic problem

We first use a one-dimensional problem with a periodic geometry size L to validate the present model for CDE and the local scheme in computing the flux. For this simple problem, one can derive its analytical solution under some suitable initial and boundary conditions [20],

$$\phi(\mathbf{x}, t) = \phi_0 + \phi_1 e^{-kD^2 t} \left\{ \cos(k\mathbf{x})\cos\left[\frac{u_0 k}{\zeta}\sin(\zeta t)\right] + \sin(k\mathbf{x})\sin\left[\frac{u_0 k}{\zeta}\sin(\zeta t)\right] \right\}, \quad (38)$$

$$\mathbf{u}(t) = u_0 \cos(\zeta t), \quad (39)$$

where $\zeta = 2\pi$, $k = 2\pi/L$, u_0, ϕ_0 and ϕ_1 are some constants; the acceleration $\mathbf{a}$ and the pressure gradient ∇P are given by

$$\mathbf{a} = -u_0 \zeta \sin(\zeta t), \quad \nabla P = 0. \quad (40)$$

From the above Eqs. (38) and (39) we can also obtain the exact solution of the flux,

$$\mathbf{J} = -D\nabla\phi + \phi\mathbf{u}$$

$$= \phi_0 u_0 \cos(\zeta t) + \phi_1 e^{-kD^2 t}\left\{[kD\sin(k\mathbf{x}) + u_0\cos(\zeta t)\cos(k\mathbf{x})]\cos\left[\frac{u_0 k}{\nu}\sin(\zeta t)\right]\right. \quad (41)$$

$$+ [u_0\cos(\zeta t)\sin(k\mathbf{x}) - kD\cos(k\mathbf{x})]\sin\left(\frac{u_0 k}{\nu}\sin(\zeta t)\right)\bigg\}$$

In simulations, the D1Q3 model (a one-dimensional model with there discrete velocities) in the lattice Boltzmann method is used. The simulations are suspended after running one period $T = 1/\zeta = N_t \delta t = 1/2\pi$ with N_t representing the time steps in one period. The parameters L, u_0, and ϕ_1 are fixed to be 1.0, while ϕ_0 is set to be 0. The numerical results at different Peléct numbers (Pe, Pe $= Lu_0/D$) and relaxation times are presented in Figs. 1 and 2. The results were obtained with a lattice size 64, which is fine enough to derive the accurate results. As seen from these two figures, the numerical results of scalar variable ϕ and the flux $\mathbf{J}$ are in good agreement with the corresponding analytical solutions.
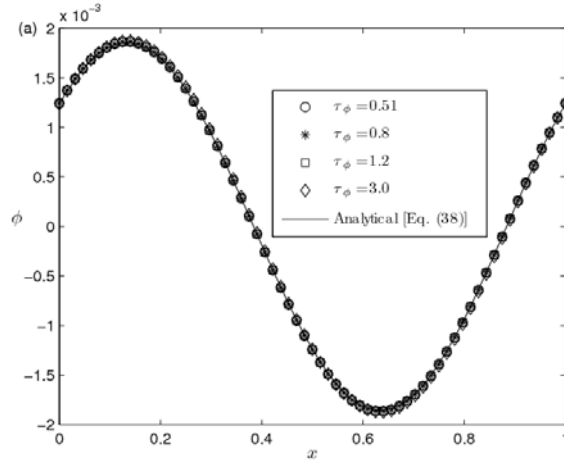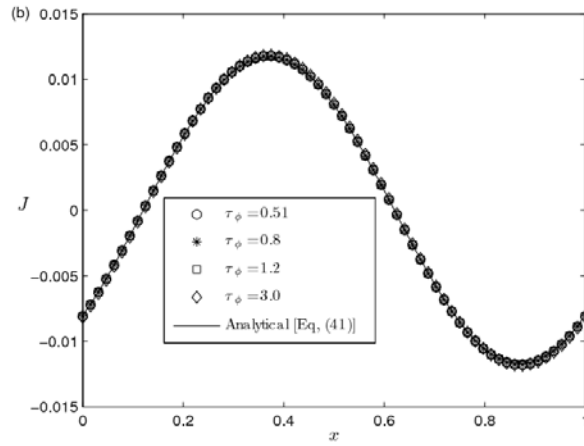
Fig. 1: The distributions of scalar variable ϕ (a) and the flux $\mathbf{J}$ (b) (Pe=1).
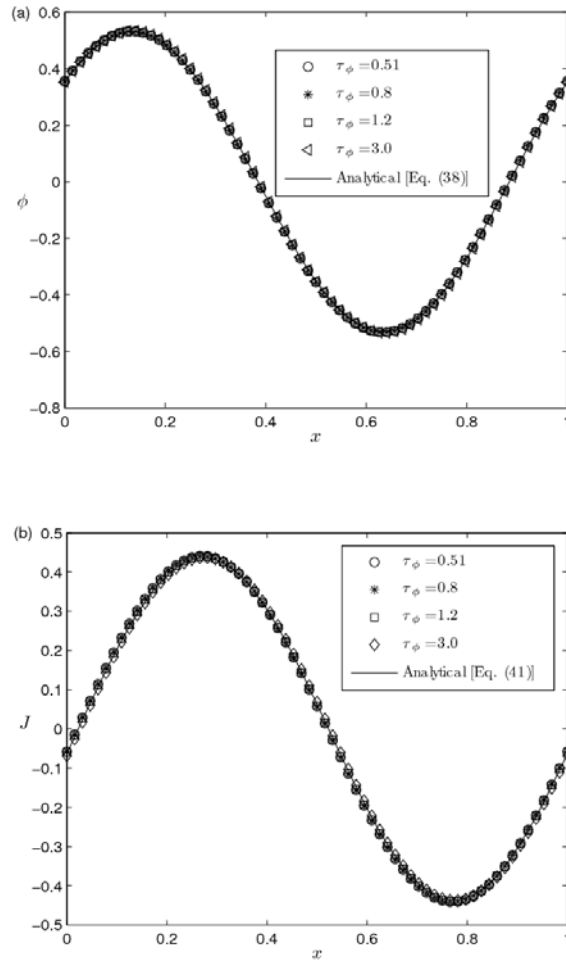
Fig. 2: The distributions of scalar variable ϕ (a) and the flux $\mathbf{J}$ (b) (Pe=10).

To quantitatively evaluate the difference between numerical results and the analytical solution, we compute the relative errors [Eq. (37)] at different Peléct numbers and relaxation times, and present the results in Tables I. As seen from this table, the results with a smaller relaxation time ($\tau_\phi = 0.51$) are comparable to those with the relaxation time near unity, which is similar to the results on shear stress [35]. However, a larger error will be obtained if the relaxation time is much larger than unity ($\tau_\phi = 3.0$). Based on these results, we can conclude that, to derive more accurate results, the relaxation time used in simulation cannot be much larger than unity.

TABLE I. Relative errors of the scalar variable ϕ and flux **J** with different relaxation times and Peléct numbers.

τ_ϕ	E_ϕ		E_J	
	Pe=1	Pe=10	Pe=1	Pe=10
0.51	1.727×10^{-3}	1.736×10^{-3}	1.019×10^{-3}	1.190×10^{-3}
0.8	1.570×10^{-3}	1.819×10^{-3}	8.659×10^{-4}	1.404×10^{-3}
1.2	8.247×10^{-4}	1.425×10^{-3}	9.814×10^{-5}	1.867×10^{-3}
3.0	1.175×10^{-2}	8.850×10^{-3}	1.222×10^{-2}	1.226×10^{-2}

In addition, we note that this problem is time-dependent, and thus it is necessary to test the error variation with the increase of time. To this end, the relative errors of scalar variable ϕ and flux **J** at different times (t) are calculated and presented in Fig. 3 where Pe=1. As seen from this figure, the relative errors of the case with a larger relaxation time ($\tau_\phi = 3.0$) increase faster in time, while there are no apparent increases for other cases. The similar results are also observed for the case of Pe=10.
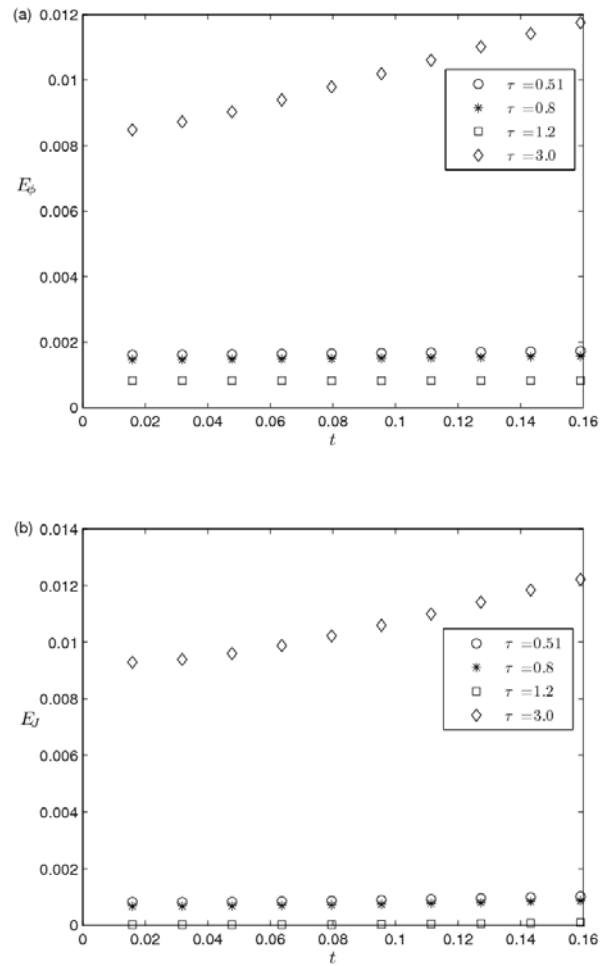
Fig. 3: The relative errors of scalar variable ϕ and flux $\mathbf{J}$ at different times.

2. The diffusion in the Couette flow with wall injection

The second tested problem is diffusion in the Couette flow with wall injection, the schematic of the problem is shown in Fig. 4, where the top and bottom walls move at different velocities u_0 and 0 in x direction, and simultaneously, a vertical velocity v_0 is injected at both walls.
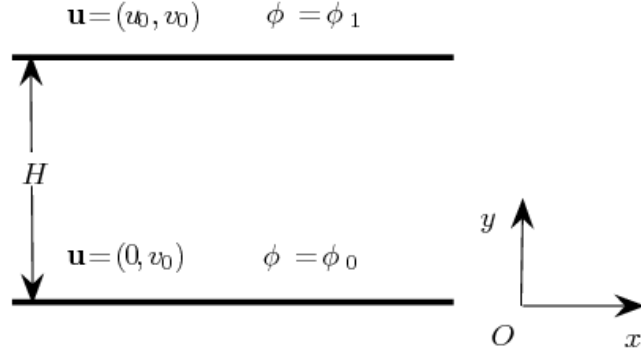
Fig. 4: Schematic of diffusion in the Couette flow with wall injection.

This problem has the following analytical solutions of velocity $\mathbf{u} = (u_x, u_y)$ and ϕ [34]:

$$u_x = u_0 \left(\frac{e^{\mathrm{Re}\frac{y}{H}} - 1}{e^{\mathrm{Re}} - 1} \right), \tag{42}$$

$$u_y = v_0, \tag{43}$$

$$\phi = \phi_0 + (\phi_1 - \phi_0) \left(\frac{e^{\mathrm{Pe}\frac{y}{H}} - 1}{e^{\mathrm{Pe}} - 1} \right), \tag{44}$$

where ϕ_0 and ϕ_1 are values of the scalar variable ϕ on the bottom and top walls, H is the height of the two-dimensional channel. Re and Pe represent the Reynolds and Peléct numbers, and defined by

$$\mathrm{Re} = \frac{Hv_0}{v}, \quad \mathrm{Pe} = \frac{Hv_0}{D}. \tag{45}$$

Based on Eqs. (42)-(45), we can also derive the analytical solution of the flux $\mathbf{J} = (J_x, J_y)$,

$$J_x = -D\frac{\partial \phi}{\partial x} + \phi u_x = u_0 \left(\frac{e^{\mathrm{Re}\frac{y}{H}} - 1}{e^{\mathrm{Re}} - 1} \right) \left[\phi_0 + (\phi_1 - \phi_0) \left(\frac{e^{\mathrm{Pe}\frac{y}{H}} - 1}{e^{\mathrm{Pe}} - 1} \right) \right], \tag{46}$$

19

$$J_y = -D \frac{\partial \phi}{\partial y} + \phi u_y = v_0 \left(\phi_0 - \frac{\phi_1 - \phi_0}{e^{\mathrm{Pe}} - 1} \right). \tag{47}$$

Several numerical experiments were performed with the D2Q9 model (a two-dimensional model with nine discrete velocities), and the parameters u_0, v_0, ϕ_0, ϕ_1, and H used in simulations were set as $u_0 = v_0 = 0.01$, $\phi_0 = 0$, $\phi_1 = 1$, and $H = 1$. We present the simulation results at different Peléct numbers in Figs. 5 and 6, in which the periodic boundary condition is applied in the horizontal direction and the lattice size is 64×64. As shown in these figures, the numerical results agree well with analytical ones, which indicates that the present model and scheme are accurate in solving CDE and computing the flux. However, we also find that, similar to the lattice BGK model for fluid flows [37], the relaxation time also influences the numerical results of this problem. Although the maximum relative error is rather small, and the value is less than 2%, an obvious deviation between the numerical and analytical results can be observed, as shown in Fig. 6(c). We also present a quantitative comparison between the numerical results and analytical solution in Table II, where the relative errors [Eq. (37)] at different Peléct numbers and relaxation times are computed. As shown in this table, the results with different relaxation times are comparable to each other. It is also found that the relative errors increase with the increase of the Peléct number, this may be due to the fact that the convection effect is more predominant at a larger Pe, which usually brings larger errors in simulations.
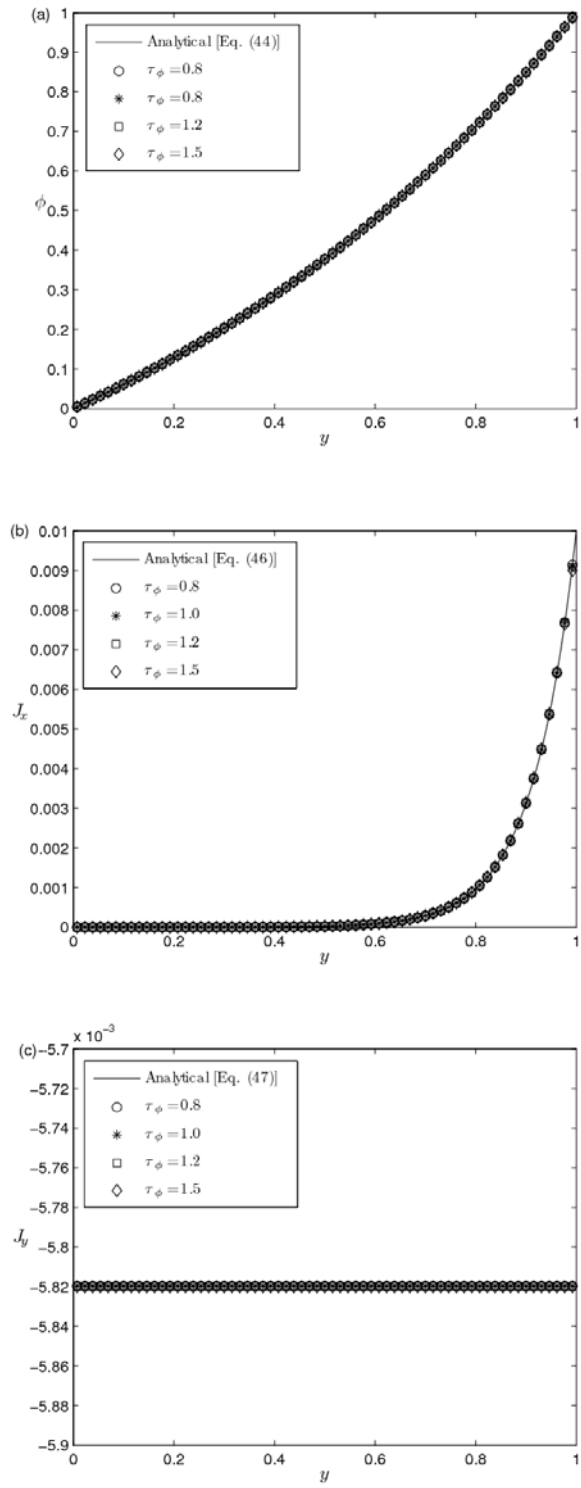
Fig. 5: The distributions of scalar variable ϕ (a) and the flux $\mathbf{J}$ (b, c) along y direction
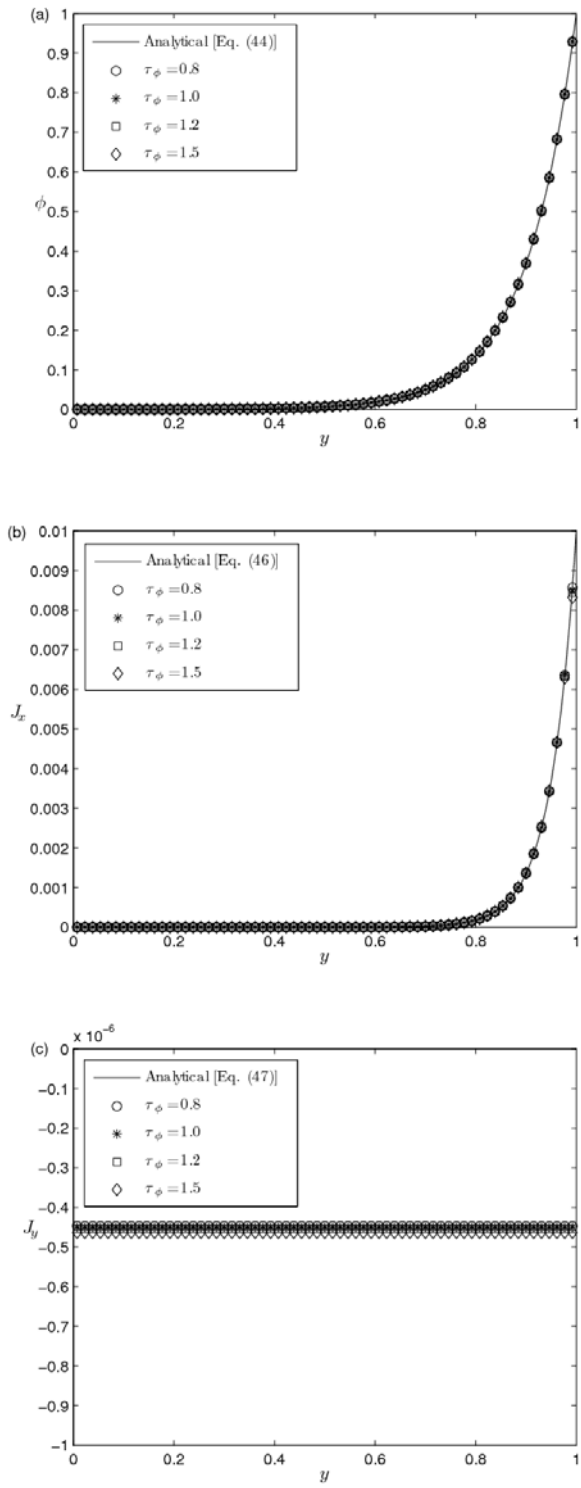
(Re=10, Pe=1).

Fig. 6: The distributions of scalar variable ϕ (a) and the flux $\mathbf{J}$ (b, c) along y direction

(Re=10, Pe=10).

TABLE II. Relative errors of the scalar variable ϕ and flux $\mathbf{J}$ with different relaxation times and Peléct numbers.

τ_ϕ	E_ϕ		E_{J_x}		E_{J_y}	
	Re=10, Pe=1	Re=10, Pe=10	Re=10, Pe=1	Re=10, Pe=10	Re=10, Pe=1	Re=10, Pe=10
0.8	6.771×10^{-5}	1.859×10^{-3}	1.861×10^{-3}	3.793×10^{-3}	2.559×10^{-5}	1.585×10^{-2}
1.0	6.891×10^{-5}	2.071×10^{-3}	2.930×10^{-3}	6.686×10^{-3}	1.560×10^{-5}	9.689×10^{-3}
1.2	7.070×10^{-5}	2.923×10^{-3}	4.134×10^{-3}	9.640×10^{-3}	6.239×10^{-7}	2.984×10^{-4}
1.5	7.452×10^{-5}	4.928×10^{-3}	6.252×10^{-3}	1.470×10^{-2}	3.120×10^{-5}	1.998×10^{-2}

3. The diffusion in the Poiseuille flow

At last, the problem of the diffusion in the Poiseuille flow is also used to test the present model for CDE and the local scheme for the flux. For this problem, the flow in the two-dimensional channel is driven by an external force $\mathbf{F} = \rho\mathbf{a} = \rho(a_x, 0)$ with constant density ρ and acceleration $\mathbf{a}$, and assumed to be periodic in horizontal direction. H is the height of the channel, ϕ_0 and ϕ_1 are the scalar variable ϕ at the top and bottom walls. Based on these boundary conditions, we can obtain theoretical solutions of the problem:

$$u_x = \frac{a_x H^2}{2\nu}\frac{y}{H}\left(1-\frac{y}{H}\right), \tag{48}$$

$$u_y = 0, \tag{49}$$

$$\phi = \phi_0 + (\phi_1 - \phi_0)\frac{y}{H}, \tag{50}$$

$$J_x = \phi u_x = \frac{a_x H^2}{2\nu}\frac{y}{H}\left(1-\frac{y}{H}\right)\left[\phi_0 + (\phi_1 - \phi_0)\frac{y}{H}\right], \tag{51}$$

23

$$J_y = -D\frac{\partial \phi}{\partial y} = -(\phi_1 - \phi_0)\frac{D}{H} . \tag{52}$$

Similar to the Problem 2, the Reynolds number and Peléct number are used, and defined as

$$\mathrm{Re} = \frac{Hu_0}{\nu}, \ \mathrm{Pe} = \frac{Hu_0}{D}, \tag{53}$$

where u_0 is the maximum velocity, and given by $u_0 = a_x H^2 / 8\nu$. After several algebraic manipulations, one can find that the Peléct number does not affect the solutions of scalar variable ϕ and flux J_x [Eqs. (50) and (51)], but it influences the solution of flux J_y.

We also used the D2Q9 model to carry out several simulations at different Peléct numbers and relaxation times; the numerical results are shown in Figs. 7 and 8. From these figures we can find that the numerical results agree well with analytical solutions. A quantitative study on the deviation between the numerical results and analytical solutions was also performed, the relative errors at different Peléct numbers and relaxation times were calculated and presented in Tables III and IV. As seen from these tables, it is found that the numerical results of scalar variable ϕ and the flux J_y almost match corresponding analytical solutions exactly, which is consistent with the theoretical analysis on this problem [34]. In addition, we also find that the relative errors of scalar variable ϕ and flux J_y decrease with the increase of relaxation time τ_g, but an opposite trend is observed for the flux J_x when the relaxation time τ_g is no less that unity. This may be because the velocity u_x in the computation of flux J_x is related to the relaxation time τ_f [37], and as a consequence depends on the relaxation time τ_g based on the relationship $\mathrm{Re}/\mathrm{Pe} = (2\tau_g - 1)/(2\tau_f - 1)$.

From the above discussion one can conclude that the relaxation time τ_g cannot be much larger in order to derive more accurate results of scalar variable ϕ and flux $\mathbf{J}$. In addition, we also would like to point out that, as the present lattice Boltzmann model and scheme are both second-order methods for scalar variable ϕ and flux $\mathbf{J}$, the numerical results should be convergent to the linear ϕ and constant flux J_y exactly. However, with an increase of Pe, the larger errors are observed, which may be caused by the fact that the convection effect predominates at a larger Pe. We also note that the errors of scalar variable ϕ and flux J_y increase dramatically when Pe is in the range from 1 to 10, while slowly as Pe is changed from 10 to 100.

25
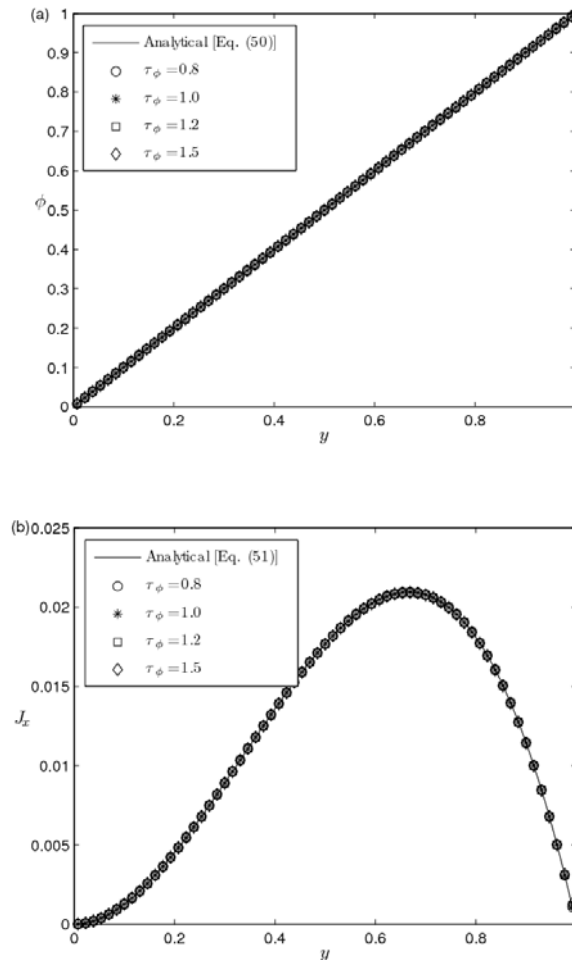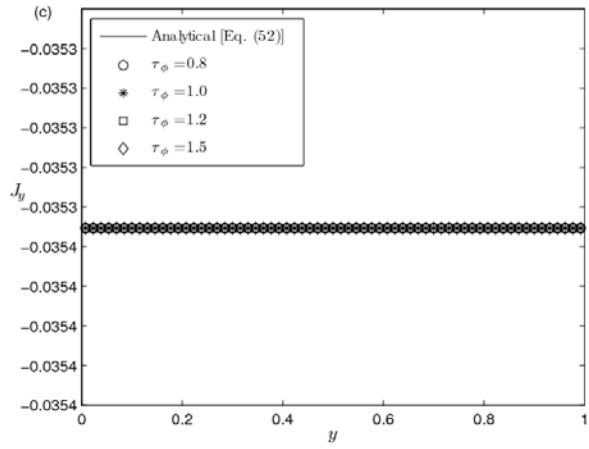
Fig. 7: The distributions of scalar variable ϕ (a) and the flux **J** (b, c) along y direction
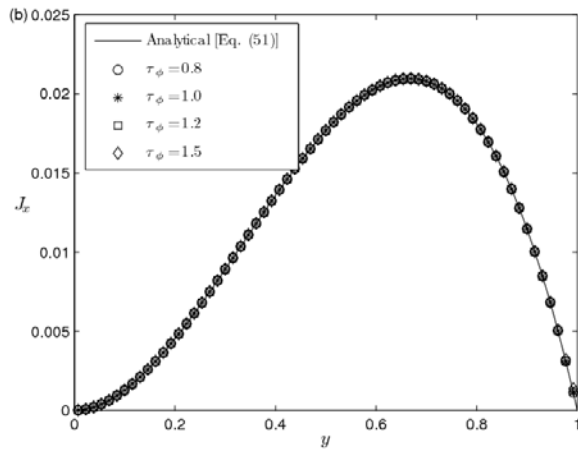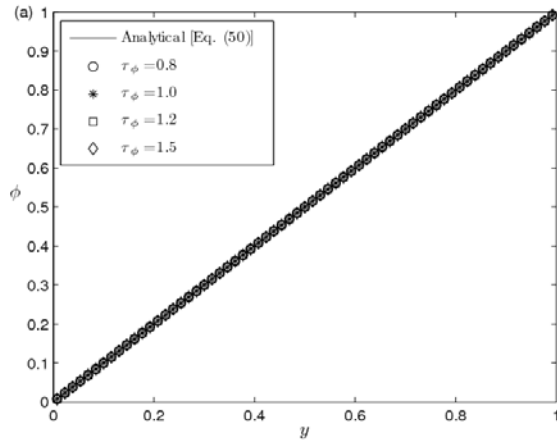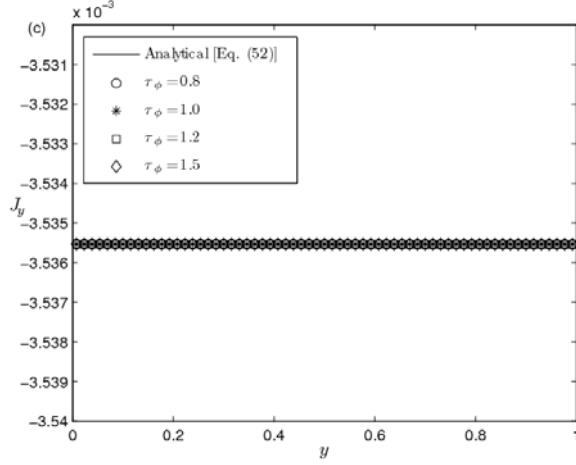
(Re=10, Pe=1).

Fig. 8: The distributions of scalar variable ϕ (a) and the flux $\mathbf{J}$ (b, c) along y direction

(Re=10, Pe=10).

TABLE III. Relative errors of the scalar variable ϕ and flux $\mathbf{J}$ with different relaxation times and Peléct numbers.

τ_ϕ	E_ϕ		E_{J_x}		E_{J_y}	
	Re=10, Pe=1	Re=10, Pe=6	Re=10, Pe=1	Re=10, Pe=6	Re=10, Pe=1	Re=10, Pe=6
0.8	4.732×10^{-13}	4.643×10^{-11}	4.445×10^{-4}	3.665×10^{-4}	1.753×10^{-12}	7.276×10^{-11}
1.0	2.337×10^{-13}	1.975×10^{-11}	5.937×10^{-4}	3.998×10^{-4}	1.179×10^{-12}	3.107×10^{-11}
1.2	1.341×10^{-13}	1.119×10^{-11}	7.919×10^{-4}	4.838×10^{-4}	1.253×10^{-12}	1.757×10^{-11}
1.5	6.988×10^{-14}	6.144×10^{-12}	1.269×10^{-3}	8.074×10^{-4}	3.620×10^{-13}	9.654×10^{-12}
3.0	9.913×10^{-15}	1.174×10^{-12}	5.502×10^{-3}	5.680×10^{-3}	2.259×10^{-14}	1.847×10^{-12}
5.0	6.584×10^{-15}	2.653×10^{-13}	1.407×10^{-2}	1.920×10^{-2}	1.610×10^{-14}	4.168×10^{-13}

TABLE IV. Relative errors of the scalar variable ϕ and flux $\mathbf{J}$ with different relaxation times and Peléct numbers.

τ_ϕ	E_ϕ		E_{J_x}		E_{J_y}	
	Re=10, Pe=10	Re=10, Pe=100	Re=10, Pe=10	Re=10, Pe=100	Re=10, Pe=10	Re=10, Pe=100

0.8	3.448×10^{-7}	4.157×10^{-7}	2.525×10^{-4}	1.711×10^{-2}	5.416×10^{-7}	6.529×10^{-7}
1.0	2.063×10^{-7}	2.507×10^{-7}	2.473×10^{-4}	4.816×10^{-2}	2.240×10^{-7}	3.936×10^{-7}
1.2	1.453×10^{-7}	1.711×10^{-7}	8.043×10^{-4}	9.473×10^{-2}	2.282×10^{-7}	2.688×10^{-7}
1.5	9.471×10^{-8}	1.196×10^{-7}	2.011×10^{-3}	1.937×10^{-1}	1.487×10^{-7}	1.879×10^{-7}
3.0	2.952×10^{-8}	4.357×10^{-8}	1.444×10^{-2}	1.213×10^{0}	4.636×10^{-8}	6.843×10^{-8}
5.0	1.419×10^{-8}	2.015×10^{-8}	4.757×10^{-2}	3.929×10^{0}	2.229×10^{-8}	3.614×10^{-8}

B. The convergence rates of the present model for the convection-diffusion equation and local scheme for computing flux

To investigate the convergence rates of the present model for CDE and the local scheme for computing the flux, the one-dimensional periodic problem described above is first used here since the boundary effect on numerical results can be excluded. We computed the relative errors with different lattice sizes, and show the results in Figs. 9 and 10. As seen from these figures, the present model for CDE is second-order accurate, as expected; more interestingly, the scheme for computing the flux also has a second-order convergence rate in space. Besides, we can also find that the relaxation time has an influence on the accuracy of the present model and the scheme for flux, but it does not affect the second-order convergence rate in space.
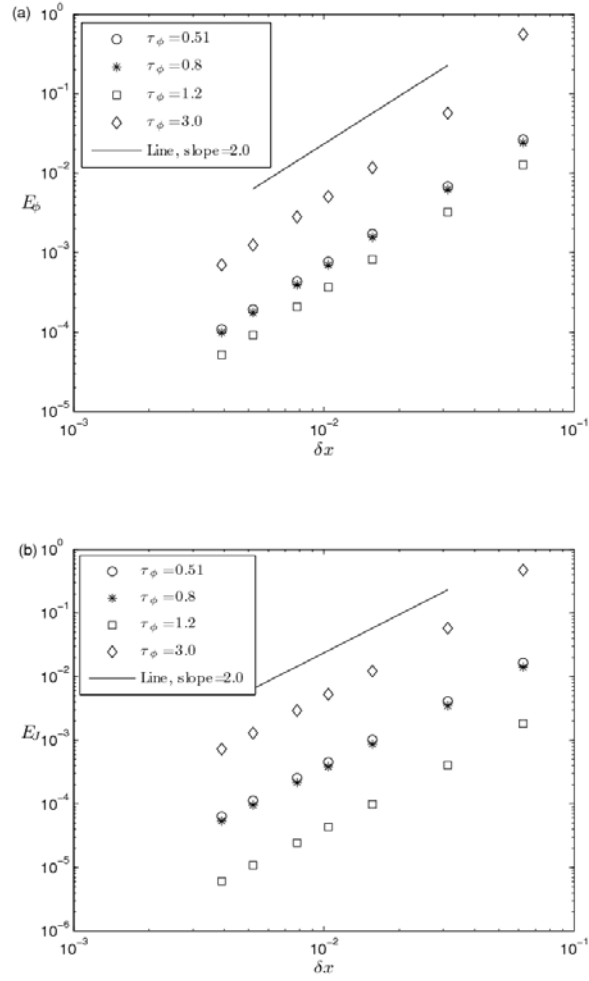
Fig. 9: The relative errors of scalar variable ϕ (a) and the flux $\mathbf{J}$ (b) at different lattice sizes ($\delta x = 1/16$, $1/32$, $1/64$, $1/96$, $1/128$, $1/192$, and $1/256$) (Pe=1). The slope of the inserted line is 2.0, which indicates the model for CDE and the scheme in computing flux have a second-order convergence rate.
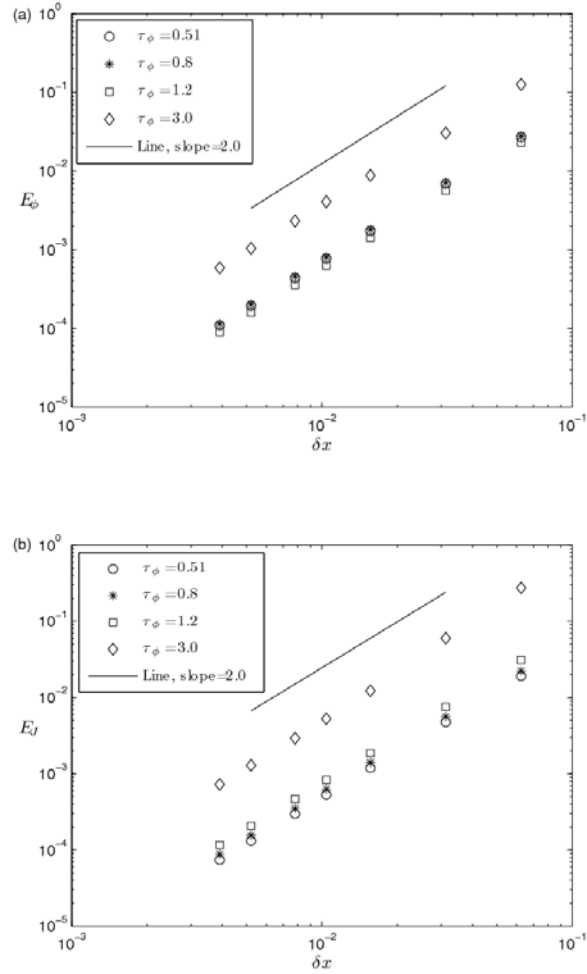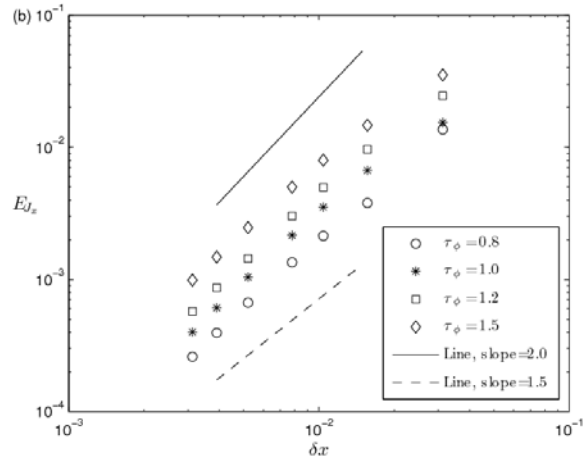
Fig. 10: The relative errors of scalar variable ϕ (a) and the flux **J** (b) at different lattice sizes ($\delta x = 1/16$, $1/32$, $1/64$, $1/96$, $1/128$, $1/192$, and $1/256$) (Pe=10). The slope of the inserted line is 2.0, which indicates the model for CDE and the scheme in computing flux have a second-order convergence rate.

Although the results presented above clearly show that the present model for CDE and the scheme in computing mass or heat flux have a second-order convergence rate, the boundary effect, which may affect the convergence rate of LBM, is not included since the periodic problem is considered. To test the boundary effect on convergence rates of the present model for CDE and the scheme for flux, we studied the problem of diffusion in

the Couette flow with wall injection at different lattice sizes, and presented the results in

Figs. 11 and 12. As shown in these figures, the appearance of the boundary does not

influence the second-order convergence rate of present model for CDE in that the half-

way anti-bounce-back scheme is a second-order method for the boundary condition of

CDE, but it affects the convergence rate of the scheme for flux [see Figs. 11(b) and

12(b)]. To see the boundary effect more clearly, the local errors of the scalar variable ϕ

$(LE_\phi = |\phi_a - \phi_n|)$ and flux J_x $(LE_{J_x} = |J_{x,a} - J_{x,n}|)$ were also computed and presented in

Fig. 13 where the lattice size and Peléct number are fixed at 64 and 10. As seen from this

figure, the larger local errors are observed near the top boundary where the scalar

variable ϕ is not zero.
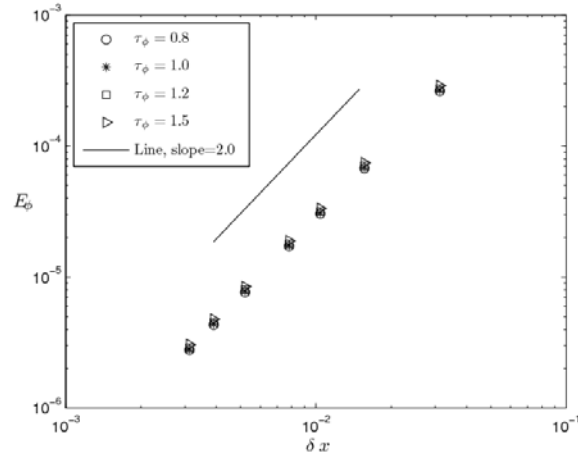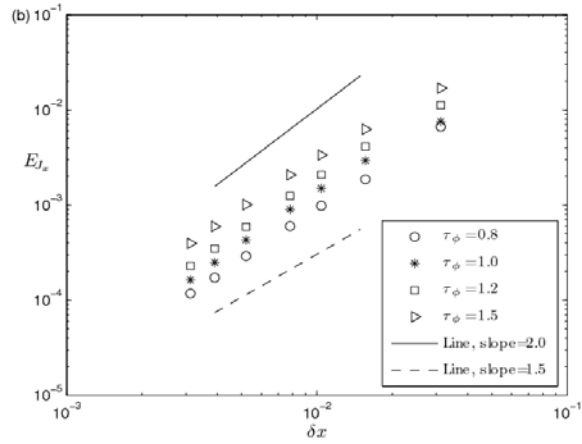
Fig. 11: The relative errors of scalar variable ϕ (a) and the flux J_x (b) at different lattice sizes ($\delta x = 1/32$, $1/64$, $1/96$, $1/128$, $1/192$, $1/256$, and $1/320$) (Re=10, Pe=1). The slope of the inserted line is used to indicate convergence rates of the model for CDE and the scheme in computing flux J_x.
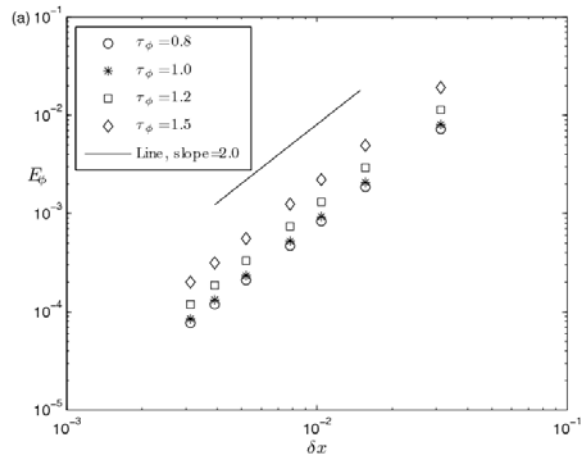
Fig. 12: The relative errors of scalar variable ϕ (a) and the flux J_x (b) at different lattice

sizes ($\delta x = 1/32$, $1/64$, $1/96$, $1/128$, $1/192$, $1/256$, and $1/320$) (Re=10, Pe=10). The

slope of the inserted line is used to indicate convergence rates of the model for CDE and

the scheme in computing flux J_x.
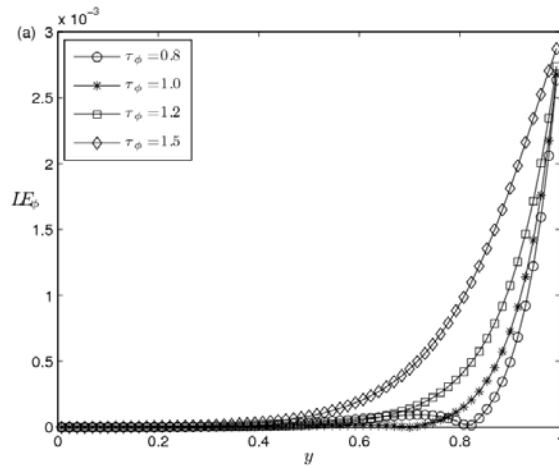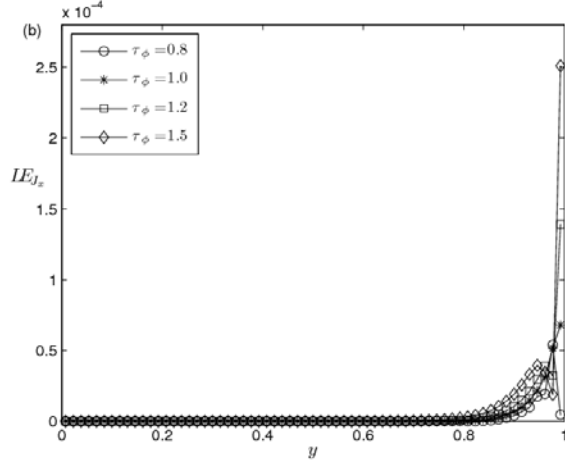
Fig. 13: The distributions of local errors of scalar variable ϕ (a) and the flux J_x (b) at

different relaxation times.

C. A comparison between the present model and previous models

The Chapman-Enskog analysis presented in Section II shows that the present model can recover the CDE correctly, which can be used to conclude that the present model should be more accurate than the popular model adopted in some previous works [10, 34]. To confirm above statement, a comparison between present model and the popular one used in Ref. [34] was conducted, and the one-dimensional periodic problem with the same parameters as those mentioned above is used in simulations. In order to give a quantitative comparison on the accuracies of these two models, the following relative difference (*RD*) between errors of the present model and the existing model is used,

$$RD = \frac{E_{\bar{\phi}} - E_{\phi}}{E_{\phi}}, \tag{54}$$

where E_{ϕ} and $E_{\bar{\phi}}$ represent the relative errors of present model and previous model. We present the relative differences at different relaxation times and lattice sizes in Fig. 14 where the Reynolds number and Peléct number are fixed to be 10 and 1. From this figure

one can find that present model is more accurate than the popular model used in Ref. [34] since the relative differences are larger than zero.
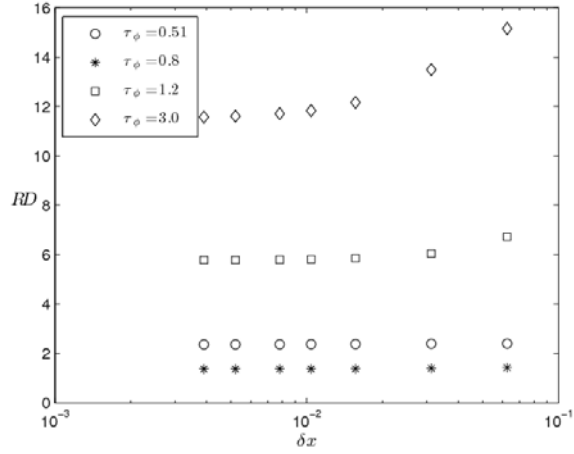
Fig. 14: The relative differences between errors of present and the previous models.

We also would like to compare the present model with the one proposed in Ref. [20] in Fig. 15. From this figure, one can find that, similar to the results shown in Fig. 14, the present model is also more accurate that the previous one [20]. And additionally, it is also found that there is no apparent difference between the results derived by the model proposed by Chopard et al. [20] and those obtained by the popular model in Ref. [34].
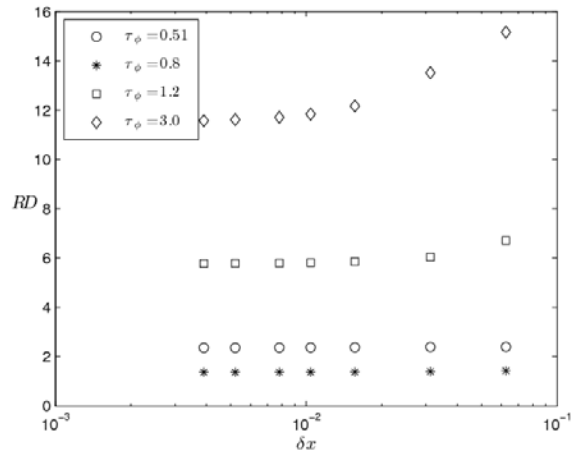
Fig. 15: The relative differences between errors of the present model and previous models.

D. An application of the present LB model: Natural convection in a square enclosure with a heated circular cylinder

A major advantage of the present model over previous models [20-22] is that the collision process can be conducted locally, and consequently, a local scheme can be constructed for the boundary conditions of CDE. To show the potential of present model in the study of the heat and mass transfer in complex geometries, the natural convection in a square enclosure with a heated circular cylinder [38, 39] was studied. A schematic of the problem is shown in Fig. 16, where a circular cylinder with a radius (R, $R = 0.2L$) and a high temperature T_h is located in the central of square enclosure with length L and a low temperature T_c, a detailed description on this problem can be found elsewhere [38, 39].
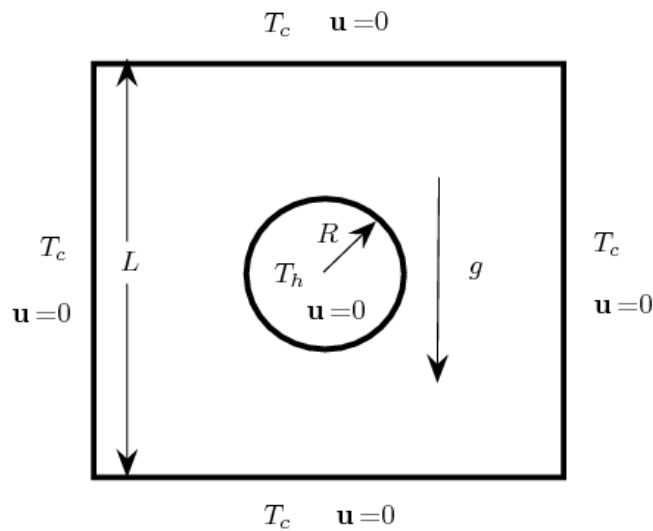
Fig. 16: Schematic of natural convection in a square enclosure with a heated circular cylinder.

In our simulations, the local boundary schemes, anti-bounce-back and bounce-back schemes, are adopted to treat the boundary conditions of temperature and flow fields; the grid number is fixed to be 512×512, which is fine enough to give grid-independence results. The Prandtl number (Pr, $\mathrm{Pr} = \nu/D$) is set to be 0.71 corresponding to that of air, and the Rayleigh number (Ra), defined by $\mathrm{Ra} = g\beta L^3 (T_h - T_c)/\nu D$ where g and β are the gravitational acceleration and volume expansion coefficient, is varied from 10^3 to 10^6. We present isothermals and streamlines in Figs. 17 and 18, and found that these results agree well with those reported in the literature [38, 39].
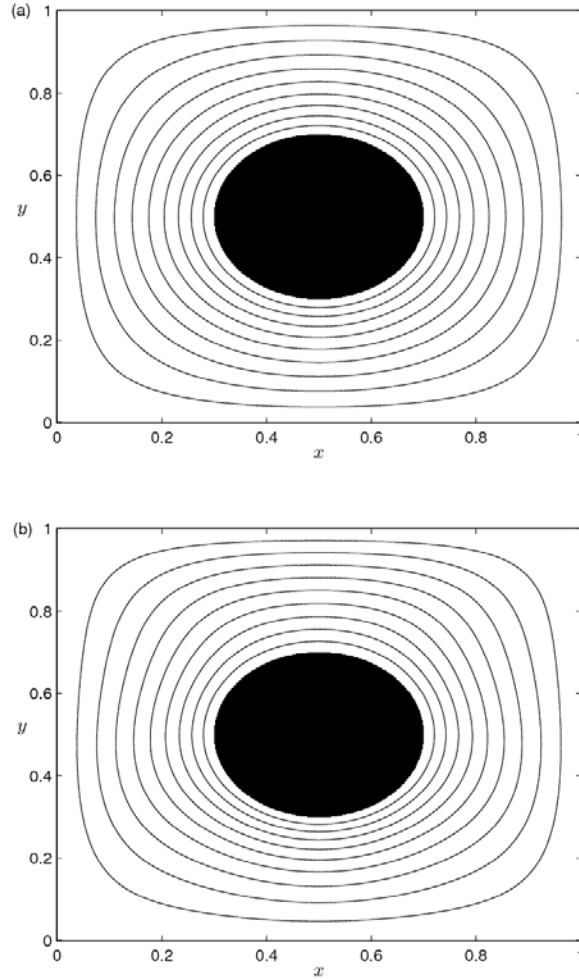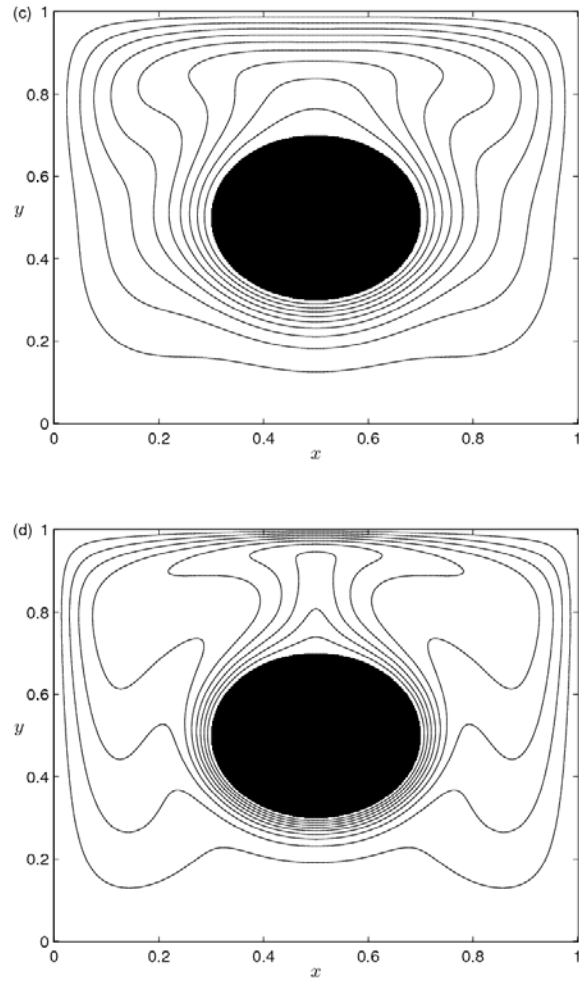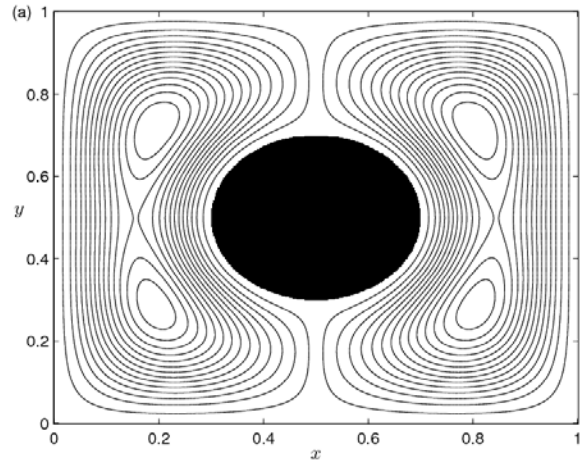
Fig. 17: Isothermals at different Rayleigh numbers; (a): Ra=10^3, (b): Ra=10^4, (c): Ra=10^5, (d): Ra=10^6.
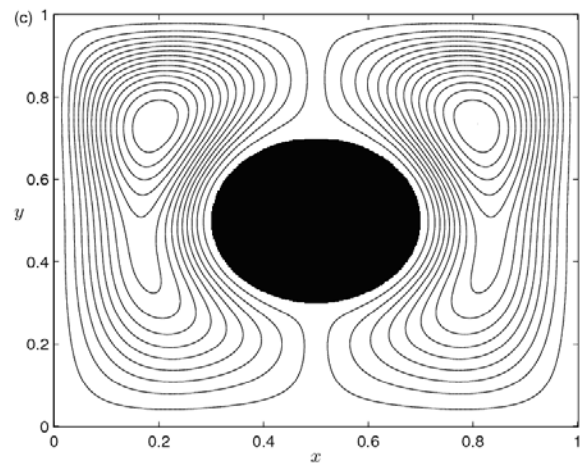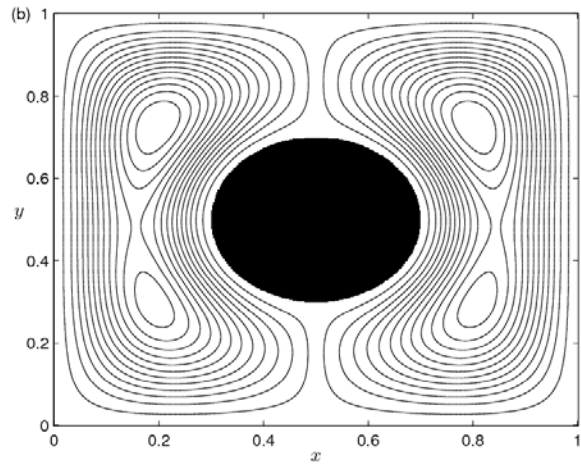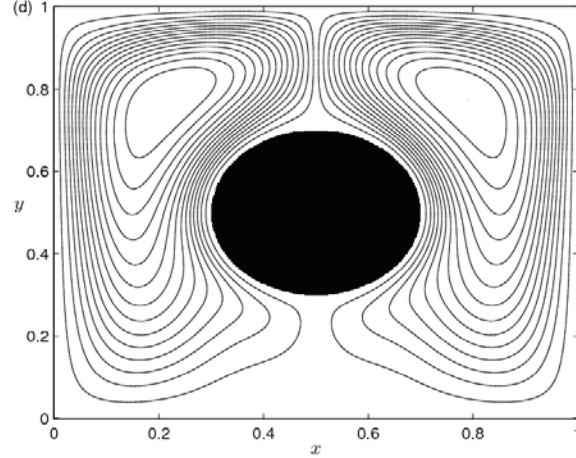
Fig. 18: Streamlines at different Rayleigh numbers; (a): Ra=10^3, (b): Ra=10^4, (c): Ra=10^5, (d): Ra=10^6.

V. Conclusion

A problem within previous LB models for the CDE is that the collision process cannot be implemented locally, which not only influences the computational efficiency of the lattice Boltzmann method, but also causes a difficulty in adopting a local scheme to treat the boundary condition of the CDE. This problem is solved by the new LB model proposed in this work. Furthermore, the present LB model enables the construction of a local scheme, instead of the traditionally nonlocal finite-difference schemes, to compute the heat and mass fluxes. The numerical validation exercises demonstrate that both the present model for the CDE and the local scheme for the flux have a second-order convergence rate in space. We also compared the present model with previous models, and found that the model proposed in this work is more accurate in solving CDE. The present work is expected to play an important role in studying heat or mass transfer processes with complex geometries.

Acknowledgments

References

[1] R. B. Bird, W. E. Stewart, and E. N. Lightfoot, *Transport Phenomena* (John Wiley & Sons, New York, 2002).

[2] J. C. Strikwerda, *Finite Difference Schemes and Partial Differential Equations* (SIAM, Philadephia, 2004).

[3] H.- G. Roos, M. Stynes, and L. Tobiska, *Robust Numerical Methods for Singularly Perturbed Differential Equations: Convection-Diffusion-Reaction and Flow Problems* (Springer, Berlin, 2008).

[4] R. Eymard, T. Gallouaet, and R. Herbin, in *Handbook of Numerical Analysis*, Vol. VII, edited by P. Ciarlet and J.-L. Lions, (Elsevier, Amsterdam, 2000), pp. 713-1018.

[5] R. Benzi, S. Succi, and M. Vergassola, Phys. Rep. **222**, 145 (1992).

[6] S. Chen and G. D. Doolen, Annu. Rev. Fluid Mech. **30**, 329 (1998).

[7] S. Succi, *The Lattice Boltzmann Equation for Fluid Dynamics and Beyond* (Oxford University press, Oxford, 2001).

[8] C. K. Aidun and J. R. Clausen, Annu. Rev. Fluid Mech. **42**, 439- 472 (2010).

[9] Q. Kang, P. C. Lichtner, and D. R. Janecky, Adv. Appl. Math. Mech. **2**, 545 (2010).

[10] S. P. Dawson, S. Chen, and G. D. Doolen, J. Chem. Phys. **98**, 1514 (1993).

[11] Z. L. Guo, B. C. Shi, and C. G. Zheng, Int. J. Numer. Methods Fluids **39**, 325 (2002).

[12] R. G. M. van der Sman and M. H. Ernst, J. Comput. Phys. **160**, 766 (2000).

[13] B. Deng, B. C. Shi, and G. C. Wang, Chin. Phys. Lett. **22**, 267 (2005).

[14] B. C. Shi, B. Deng, R. Du, and X. W. Chen, Comput. Math. Appl. **55**, 1568 (2008).

[15] X. Zhang, A. G. Bengough, J. W. Crawford, I. M. Young, Adv. Water Resour. **25**, 1 (2002).

[16] I. Ginzburg, Adv. Water Resour. **28**, 1171 (2005).

[17] I. Ginzburg, Adv. Water Resour. **28**, 1196 (2005).

[18] I. Rasin, S. Succi, and W. Miller, J. Comput. Phys. **206**, 453 (2005).

[19] H. Yoshida and M. Nagaoka, J. Comput. Phys. **229**, 7774 (2010).

[20] B. Chopard, J. L. Falcone, and J. Latt, Eur. Phys. J. **171**, 245 (2009).

[21] H.- B. Huang, X.- Y. Lu, and M. C. Sukop, J. Phys. A: Math. Theor. **44**, 055001 (2011).

[22] H. W. Zheng, C. Shu, and Y. T. Chew, J. Comput. Phys. **218**, 353 (2006).

[23] G. Yan, J. Comput. Phys. **161**, 61 (2000).

[24] Z. Chai, B. Shi, and L. Zheng, Chaos, Solitons, Fractals **36**, 874 (2008).

[25] B. Shi and Z. Guo, Phys. Rev. E **79**, 016701 (2009).

[26] V. Yermakou and S. Succi, Phys. A **391**, 4557 (2012).

[27] Y. H. Qian, D. d'Humires, and P. Lallemand, Europhys. Lett. **17**, 478 (1992).

[28] I. Ginzbourg, F. Verhaeghe, and D. d'Humieres, Commun. Comput. Phys. **3**, 427 (2008).

[29] D. d'Humieres, in *Rarefied Gas Dynamics: Theory and Simulations*, Vol. 159 of Progress in Astronautics and Aeronautics, edited by B. D. Shizgal and D. P. Weave, (AIAA, Washington, DC, 1992), pp. 450-458.

[30] P. Lallemand and L.-S. Luo, Phys. Rev. E **61**, 6546 (2000).

[31] X. He and L.-S. Luo, J. Stat. Phys. **88**, 927 (1997).

[32] Z. Guo, C. Zheng, and B. Shi, Phys. Rev. E **65**, 046308 (2002).

[33] M. Wang and N. Pan, Mater. Sci. Eng. R **63**, 1 (2008).

[34] T. Zhang, B. Shi, Z. Guo, Z. Chai, and J. Lu, Phys. Rev. E **85**, 016701 (2012).

[35] T. Kruger, F. Varnik, and D. Raabe, Phys. Rev. E **79**, 046704 (2009); **82**, 025701 (2010).

[36] Z. Chai and T. S. Zhao, Phys. Rev. E **86**, 016705 (2012).

[37] X. He, Q. Zou, L.-S. Luo, and M. Dembo, J. Stat. Phys. **87**, 115 (1997).

[38] F. Moukalled and S. Acharya, J. Thermophys. Heat Transf. **10**, 524 (1996).

[39] B. S. Kim, D. S. Lee, M. Y. Ha, and H. S. Yoon, Int. J. Heat Mass Transf. **51**, 1888 (2008).